

Webly-Supervised Image Manipulation Localization via Category-Aware Auto-Annotation

Chenfan Qu, Yiwu Zhong, Bin Li *Senior Member, IEEE*, Lianwen Jin *Member, IEEE*,

Abstract—Images manipulated using image editing tools can mislead viewers and pose significant risks to social security. However, accurately localizing the manipulated regions within an image remains a challenging problem. One of the main barriers in this area is the high cost of data acquisition and the severe lack of high-quality annotated datasets. To address this challenge, we introduce novel methods that mitigate data scarcity by leveraging readily available web data. We utilize a large collection of manually forged images from the web, as well as automatically generated annotations derived from a simpler auxiliary task, constrained image manipulation localization. Specifically, we introduce a new paradigm CAAAv2, which automatically and accurately annotates manipulated regions at the pixel level. To further improve annotation quality, we propose a novel metric, QES, which filters out unreliable annotations. Through CAAAv2 and QES, we construct MIMLv2, a large-scale, diverse, and high-quality dataset containing 246,212 manually forged images with pixel-level mask annotations. This is over 120× larger than existing handcrafted datasets like IMD20. Additionally, we introduce Object Jitter, a technique that further enhances model training by generating high-quality manipulation artifacts. Building on these advances, we develop a new model, Web-IML, designed to effectively leverage web-scale supervision for the image manipulation localization task. Extensive experiments demonstrate that our approach substantially alleviates the data scarcity problem and significantly improves the performance of various models on multiple real-world forgery benchmarks. With the proposed web supervision, Web-IML achieves a striking performance gain of 31% and surpasses previous state-of-the-art TruFor by 24.1 average IoU points. The dataset and code will be made publicly available at <https://github.com/qcf-568/MIML>.

Index Terms—Image manipulation localization, automatic annotation, web supervision, image forensics.

I. INTRODUCTION

THE misuse of manipulated images can lead to fraud and the spread of misinformation, posing serious threats to social media security [1]. To this end, Image Manipulation Localization (IML) has gained increasing attention in recent years as a critical research problem [2], [3]. A central challenge in IML lies in the scarcity of large-scale high-quality data [4], which is essential for preventing model overfitting. Generating such data is extremely labor-intensive and time-consuming [5], [6]. It requires not only crafting convincing manipulated images but also providing precise pixel-level

This research is supported in part by NSFC (Grant No.: 62476093) and GD-NSF (No.2021A1515011870). (Corresponding author: Lianwen Jin.)

Chenfan Qu and Lianwen Jin are with the DLVC-Lab of South China University of Technology, Guangdong 510641, China. (Email: 202221012612@mail.scut.edu.cn, eelwj@scut.edu.cn)

Yiwu Zhong is with the Peking University, Beijing 100091, China. (Email: yiwu-zhong@outlook.com)

Bin Li is with the College of Electronic and Information Engineering, Shenzhen University, Shenzhen 518060, China. (Email: libin@szu.edu.cn)

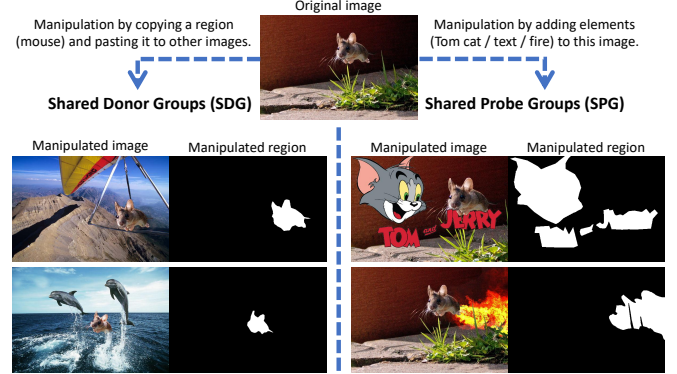


Fig. 1. When an image is tampered with by copy-pasting foreground objects from original images, the resulting original-tampered image pair belongs to Shared Donor Group (SDG). When an image is forged by directly modifying elements in place, the pair belongs to Shared Probe Group (SPG).

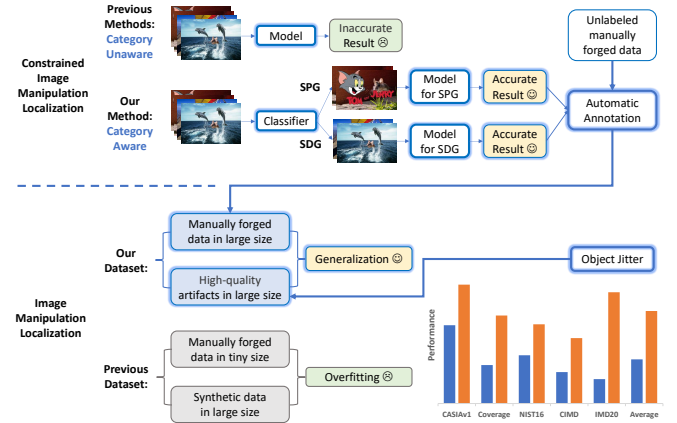


Fig. 2. We propose a novel CIML method that processes the SPG and SDG images separately. It is used for automatic annotation, constructing a large-scale, high-quality dataset. The dataset notably enhances the generalization of image manipulation localization models. Additionally, the Object Jitter method is introduced to further enlarge the dataset size and data diversity.

annotations of the forged regions. Synthetic data has been explored as an alternative [7], [8], but the resulting images often differ substantially from real-world forgeries, creating a significant domain gap that hinders model generalization [4]. Recent methods have attempted to close this gap by leveraging noise domain features [9], [10] and semantic suppression techniques [6], showing progress in improving robustness. Nevertheless, these methods do not fully resolve the fundamental issue: the lack of large-scale, manually forged data. As a result, overfitting remains a persistent challenge in IML.

Meanwhile, there are abundant manually forged images publicly available on the web, often accompanied by their corresponding originals. We propose to leverage such resources

to address the data scarcity problem in IML. Specifically, we propose leveraging Constrained Image Manipulation Localization (CIML) models to automatically generate pixel-level mask annotations for these unlabeled forged images. Our key insight is that CIML simplifies the manipulation localization task by comparing a forged image with its corresponding original. This reduction in task complexity allows CIML to produce more accurate and reliable annotations for real-world manipulations. As a result, CIML offers a practical solution for automatically generating large-scale, high-quality training datasets for IML.

However, despite recent progress on less challenging data, existing CIML methods remain inadequate as reliable automatic annotators for complex real-world images, due to three major limitations. **First**, most prior approaches rely on a single correlation-based model to handle all input data [11], [12], which we argue is a suboptimal design. In practice, image pairs consisting of forged images and their corresponding original images can be categorized into two distinct types based on their relationship (see Fig. 1): (1) Shared Donor Group (SDG), where forged image is created by copying objects from the original image and pasting them onto another image. In SDG, the shared content between the real and fake images is the foreground object. (2) Shared Probe Group (SPG), where forged image is created by directly modifying the original image. In SPG, the shared content is the less object-specific background. Although correlation-based methods work reasonably well on SDG data, they are less effective on SPG data. This is because the shared backgrounds in SPG cover larger areas and offer fewer discriminative features compared to the localized, distinctive foregrounds in SDG. Training a single correlation model on both groups can therefore lead to confusion, resulting in degraded generalization and performance. **Second**, existing CIML methods overlook an important signal, that is the difference maps obtained by subtracting forged images from their originals. These difference maps consistently highlight manipulated regions and offer strong localization cues on SPG data. However, previous studies did not treat SPG and SDG images separately, thereby leaving this valuable signal underutilized. **Third**, CIML on SDG is inherently much more challenging than on SPG. Unlike SPG, CIML on SDG cannot benefit from image difference information. Additionally, SDG exhibits greater visual complexity and diverse manipulation patterns. Unfortunately, high-quality training data for SDG is extremely limited, making it difficult to train robust and generalizable models for real-world scenarios.

To tackle these problems, we propose a novel paradigm termed as Category-Aware Auto-Annotation v2 (CAAav2), which treats image pairs in SDG and SPG separately. Our CAAav2 comprises three components. At the beginning, a classifier is employed to determine whether an input image pair belongs to SDG or SPG. This classifier can be trained effectively through self-supervised learning using unlabeled images. Moving forward, a Difference-Aware Semantic Segmentation model that utilizes both the image pairs and their difference maps for accurate constrained manipulation localization in SPG. Additionally, a Correlation DINO model that improves generalization on SDG with a frozen DINOv2 [13] encoder, a Learnable Aggregation module, a Feature Super

Resolution module and a Multi-Aspect Denoiser.

The proposed CAAav2 is **an upgraded version of our CAAA at CVPR 2024** [14]. In our earlier work, overfitting occurred in SDG because a trainable backbone was used during training with limited data. To address this issue, we now employ a frozen ViT backbone, which has resulted in significant improvements for CIML on SDG.

Subsequently, we collect a large amount of manually forged images from the Internet and then annotate their forged regions with the proposed CAAav2. This approach considerably alleviates the data scarcity in image manipulation localization. To ensure the reliability of the annotations, we propose Quality Evaluation Score (QES), a novel metric that automatically evaluates annotation quality and filters out inadequate ones. Experiments demonstrate that our MIMLv2 dataset significantly improves generalization of various models on widely used benchmarks, as shown in Fig. 2.

Furthermore, the enhanced precision of CAAav2 ensures that a greater number of high-quality samples are retained after filtering. Consequently, **MIMLv2 is both larger and more diverse than our conference version MIMLv1** [14], better supporting the development of IML models.

To further enhance the scale and diversity of web supervision, we propose Object Jitter. This method generates semantically reasonable high-quality artifacts by introducing slight distortions to random objects, such as enlargement, overexposure, or texture alteration. Then, we train IML models to localize these distorted objects. Our approach effectively supplements MIMLv2 with additional authentic web images. **This also differs from our conference paper that only uses MIMLv1 dataset to improve IML models.**

To best leverage our high-quality web-scale supervision for IML, we further propose a new model named Web-IML. It comprises an encoder, a Multi-Scale Perception module, and a Self-Rectification module. The Multi-Scale Perception module enables the model to better integrate information from multiple perspectives. The Self-Rectification module allows the model to learn to identify and correct its mistakes. Our Web-IML significantly outperforms previous methods on various widely used benchmarks, **being smaller yet more effective than the APSC-Net in our conference version.**

In summary, our main contributions are as follows:

- We propose to address the challenging IML task through the abundant web forgeries and their high-quality annotations distilled from a less challenging task, CIML.
- We introduce a novel method **CAAav2** for CIML, along with a novel metric QES designed to assess prediction quality. Together, they are used to automatically annotate manually forged web images, constructing a large-scale, diverse, high-quality dataset **MIMLv2**. This dataset considerably alleviates the data scarcity in IML.
- To further increase the size and diversity of the training data, we introduce Object Jitter, which generates high-quality artifacts using authentic web images.
- We design a new model Web-IML, to better leverage the web-scale supervision. Extensive experiments have confirmed the effectiveness of the proposed method.

Category-Aware Auto-Annotation v2 (CAAav2)

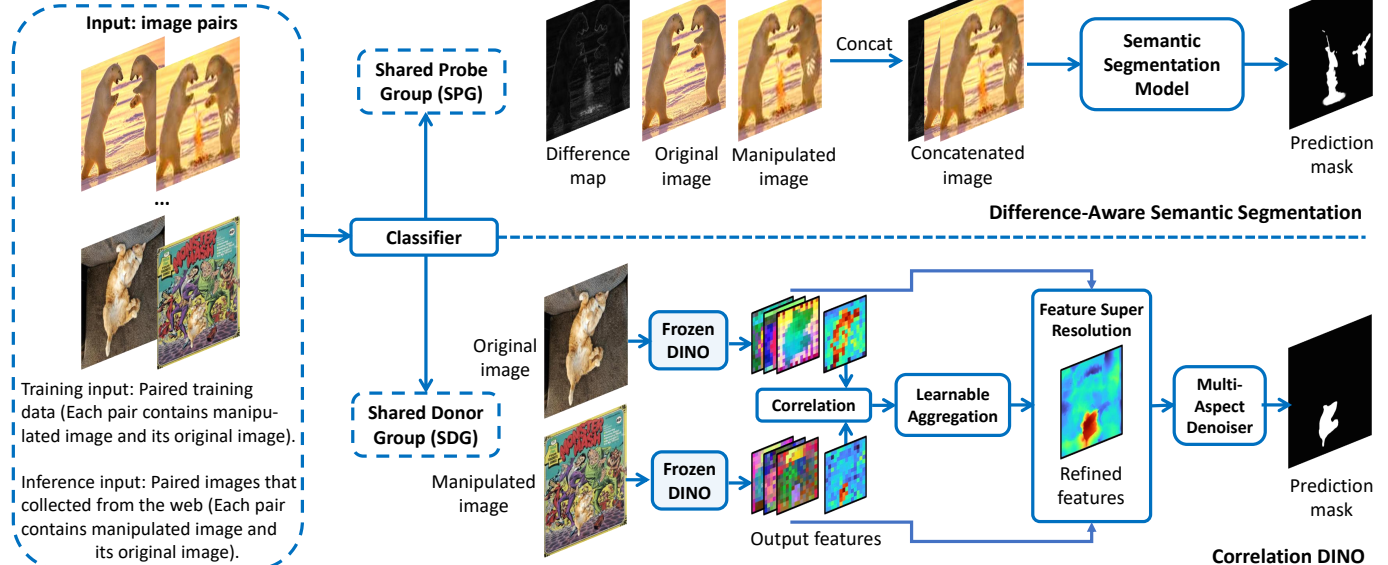


Fig. 3. The overall pipeline of our proposed CAAv2 paradigm. The input original-manipulated image pairs are first fed into a classifier to be classified into SPG or SDG. Then, we use Difference Aware Semantic Segmentation and Correlation DINO to predict forged regions in SPG and SDG respectively.

II. RELATED WORKS

Image Manipulation Localization aims to identify forged regions within images [15]–[19]. Due to costly data collection, existing handcrafted datasets are tiny in size, leading to overfitting in many models [4], [6]. To address overfitting, some studies incorporated handcrafted features. RGB-N [9] utilized SRM [9] filters to suppress semantic bias. MVSS-Net [20] and MGQFormer [21] further exploited learnable noise domain modeling. CAT-Net [7], ObjectFormer [22] and HiFi-Net [23] leveraged frequency features to localize manipulations. However, the handcrafted features are mostly noisy and unstable, hindering further improvements in model performance. Recently, pure vision models with semantic suppression techniques have achieved better performance [24], [25]. NCL [4] employed contrastive learning to improve generalization. SparseViT [6] utilized dilated attention to reduce semantic bias. Despite the progress made, these works still suffer a lot from over-fitting due to scarce high-quality data. To this end, we propose to address data scarcity by constructing a large-scale high-quality dataset, with the Internet images accurately annotated in an automatic way.

Constrained Image Manipulation Localization aims at identifying the forged image region with reference to its original image [26]. Most prior works relied on correlation matching and treated SDG and SPG image pairs uniformly. DMVN [26] computed correlation maps to localize similar objects across image pairs. DMAC [11] incorporated dilated convolution for enhanced spatial information. AttentionDM [12] employed attention mechanism for better performance. MSTAF [27] performed correlation in both the encoder and decoder to extract better features. While these methods achieved notable progress on less challenging datasets (e.g., synthetic COCO [26]), their performance is limited in real-world scenarios characterized by high resolution, large variations, and complex details. In contrast to previous approaches, our method treats SPG and

SDG separately, leveraging the differences between forged images and their originals. We are also the first to employ a frozen backbone for this task, effectively reducing overfitting.

III. CATEGORY-AWARE AUTO-ANNOTATION V2

For constrained image manipulation localization (CIML), previous works didn't consider the critical discrepancy between SPG and SDG images, and processed them using a single correlation-based model. We argue that such a paradigm is sub-optimal and the reasons are as follows:

First, the similar regions in SDG images are typically foreground objects (e.g., the cats in the SDG branch of Fig. 3) that have specific, similar shapes and distinctive features. In contrast, the similar regions in SPG images are background, which generally lacks distinctive features for accurate correlation matching (e.g., for the images of the SPG branch in Fig. 3, a patch of snow in the background is similar to all other snow patches). These background regions will cause confusion for correlation-based models, especially in complex scenarios.

Second, the difference between the forged image and its original in an SPG pair serves as an important cue. Most areas in an SPG image pair are almost identical and spatially aligned (e.g., the image pair in the SPG branch of Fig. 3). Simply subtracting between them yields a difference map that can always highlight the manipulated regions. However, this information is difficult to utilize in correlation-matching-based models and was therefore overlooked in prior works.

Based on these observations, we propose a novel paradigm for the CIML task, Category-Aware Auto-Annotation v2 (CAAav2). **The key idea is to process SPG and SDG images independently**, as shown in Fig. 3. First, a classifier (described in Section III.A) categorizes the input image pairs as either SPG or SDG. For SPG pairs, we apply Difference-Aware Semantic Segmentation (Section III.B). For SDG pairs, we process the images using Correlation DINO (Section III.C).

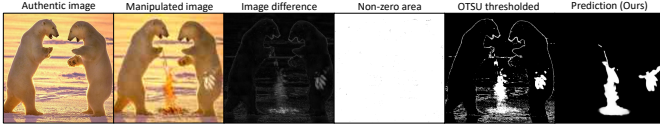


Fig. 4. Manipulated images often degrade during transmission. As a result, the absolute difference between a tampered image and its original does not accurately indicate the forged region. Our method effectively denoises the difference map by leveraging semantic information.

Importantly, the trained models are further used to auto-annotate unlabeled forged images, thereby addressing the data scarcity issue in IML tasks.

The difference between CAAAv2 and its conference version CAAA lies in the SDG branch model. In CAAA, we processed SDG image pairs using a trainable CNN structure, which tended to overfit the limited training data. In contrast, CAAAv2 employs a well pre-trained frozen ViT backbone, thereby reducing overfitting to task-specific data. Moreover, the ViT backbone naturally integrates global information, thereby alleviating semantic misalignment caused by scale diversity.

A. Self-Supervised Classification

To achieve the classification of SPG and SDG, we propose training a classifier via self-supervised learning on unlabeled images. Given an image, we apply random augmentations (e.g. color jitter, image compression) and manipulations (copy-paste, splicing or removal). The manipulated image and the original image form an SPG pair. To construct an SDG pair, we copy 1-3 random regions from the original image, resize them, and paste them into another image. With the obtained image pairs, we can effectively train our classifier. Our classifier actually only needs to discern whether the main area of the input image pair is identical or not, without considering which image or region is fake. For example, in Fig. 8, the two images in any SPG pair are nearly identical and spatially aligned, whereas images in any SDG pair are distinctly different. These characteristics are universally applicable and strong enough. Therefore, this classification task is quite simple, enabling accurate separation of images into the two groups.

B. Difference-Aware Semantic Segmentation (DASS)

Ideally, for an SPG image pair, the absolute difference between the authentic and forged images would directly reveal the forged region. However, due to transmission noise and image degradation [28], the absolute difference map is often imprecise. As shown in Fig. 4, almost every area in the difference map shows nonzero values because of noise. Even after binarizing the difference map using an OTSU [29] adaptive threshold, noisy highlights persist, especially in high-frequency regions such as edges. To address this issue, we propose **denoising the difference map by incorporating semantic information from the images**. Specifically, we concatenate the authentic image, the forged image, and their absolute difference map along the channel dimension, and feed the result into a semantic segmentation model. Our segmentation model employs a VAN [30] encoder for semantic feature extraction and utilizes the same Multi-Aspect Denoiser as in our Corr-DINO to denoise the difference map.

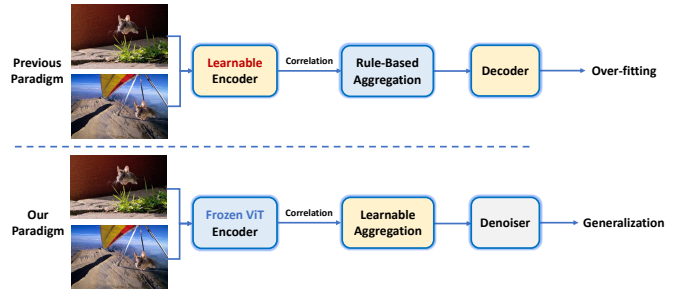


Fig. 5. Different from previous works that employ learnable encoders and rule-based feature aggregation for constrained image manipulation localization on SDG image pairs, we propose a novel frozen-denoising paradigm. This paradigm offers significantly better generalization in real-world scenarios.

C. Correlation DINO (Corr-DINO)

CIML on SDG requires detecting shared objects at various scales within complex backgrounds. This task is considerably more challenging than SPG, where targets are already highlighted through image difference maps. As a result, synthetic or small-scale handcrafted datasets are largely insufficient for training a robust model for complex real-world scenarios.

To tackle the overfitting issue, we introduce a novel frozen-denoising paradigm (see Fig. 5). **Our key insight is that overfitting can be mitigated by employing a frozen encoder and subsequently denoising its output features.** Building on this paradigm, we developed the Corr-DINO model (see Fig. 6), which consists of five components:

1. **Frozen Encoder** for feature extraction. We extract features from both the tampered image I_a and its original image I_b with a frozen DINOv2 [13] backbone. This ViT backbone has learned generalized representations through self-supervised learning on vast-scale web images. The features from the last ViT layer, denoted as F_{a1} and F_{b1} , contain rich semantic information and are used to compute correlation features.
2. **Correlation** module for correlation features calculation. $F_{a_corr} = [Corr(F_{a1}, F_{b1}), Corr(F_{a1}, F_{a1})]$, $F_{b_corr} = [Corr(F_{b1}, F_{a1}), Corr(F_{b1}, F_{b1})]$. The same correlation function $Corr$ as most previous works [12], [14], [27] is adopted. The detailed $Corr$ function is presented in the Appendix.
3. A **Learnable Aggregation** module for dimension reduction. Previous works simply select the top-K activated channels with the highest average values in F_{a_corr} and F_{b_corr} to reduce dimension. This approach works for trainable encoders but is suboptimal for our frozen encoder, whose correlated object features are relatively sparse. Selecting only the top-K channels may discard important features and compromise the integrity of F_{a_corr} and F_{b_corr} . To overcome this, we propose a learnable aggregation module that uses trainable parameters to reduce the channel count to K. Following prior methods, we also include statistics such as average and maximum values across the channel dimension. $F_{a_aggr} = [C_{1 \times 1}(R(C_{1 \times 1}(F_{a_corr}))), Avg(F_{a_corr}), Max(F_{a_corr})]$. Here, $C_{1 \times 1}$ is 1×1 conv-layer and R is ReLU. A similar process is used for F_{b_corr} to generate F_{b_aggr} .
4. **Feature Super Resolution** module for image detail reconstruction. The features from the last ViT layer are rich in

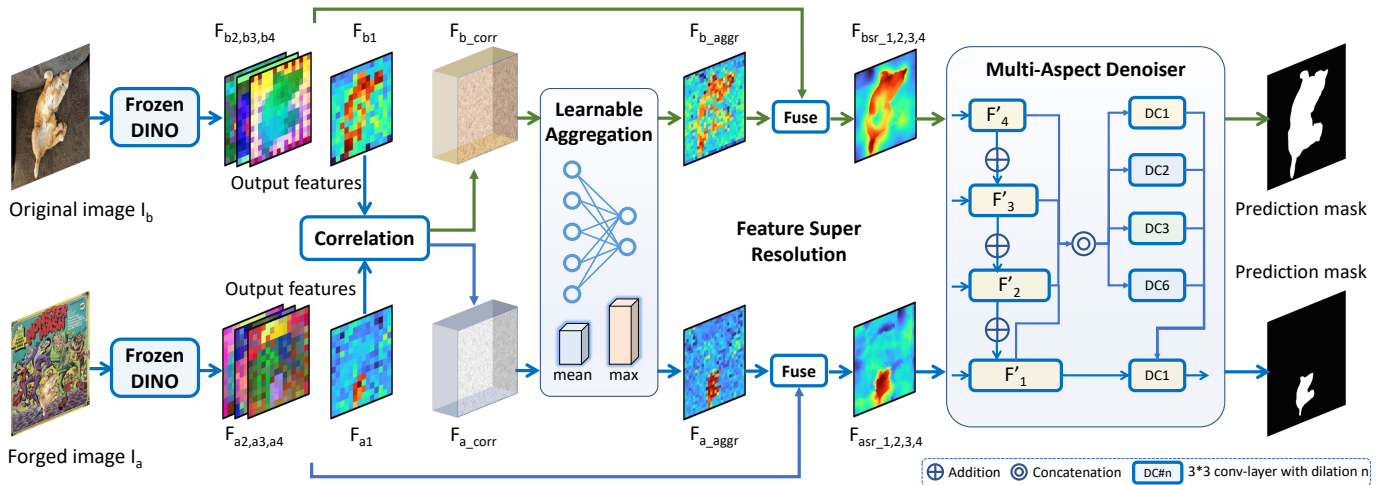


Fig. 6. The overall pipeline of our proposed Correlation DINO. First, we employ a frozen DINO backbone to extract image features. The features obtained from the final DINO layer are then used for correlation calculation. Next, a learnable aggregation module reduces the channel dimension of the correlation features, which are further refined using a Feature Super Resolution module. Finally, the refined features are denoised with a Multi-Aspect Denoiser, resulting in the final mask prediction. Green lines indicate operations used only during training with synthetic data, due to the lack of mask labels for the real images.

semantics but lack fine image details [13], making F_{a_aggr} and F_{b_aggr} too coarse for fine-grained mask predictions. To reconstruct image details, we leverage features from the last 2-4 layers of DINO, which are known to be more sensitive to edges and fine details [13]. We concatenate the features from the last four encoder layers $F_a = \text{Concat}(F_{a1,2,3,4})$ and interpolate F_{a_aggr} to different scales ($1\times, 2\times, 4\times, 8\times$) to obtain $F_{aggr_a1,2,3,4}$. We then fuse them with 1×1 conv-layers. $F_{asr_i} = \text{Conv}_{1\times 1}(\text{Conv}_{1\times 1}(F_a) + \text{Conv}_{1\times 1}(F_{aggr_ai}))$ for $i \in \{1, 2, 3, 4\}$. A similar process is applied to F_{b_aggr} .

5. Multi-Aspect Denoiser module for features denoising. Since the ViT encoder is frozen, its output features inevitably contain significant task-irrelevant noise. To achieve precise mask prediction, we propose denoising the correlation features by integrating multi-perspective information. This module fuses multi-scale features $F_{asr_1,2,3,4}$ in a top-down manner. $F'_4 = \text{Conv}_{3\times 3}([F_{asr_4}, \text{Avg}(F_{asr_4})])$, $F'_n = \text{Conv}_{3\times 3}(F'_{n+1} + \text{Conv}_{1\times 1}(F_{asr_n}))$ for $i \in \{1, 2, 3\}$. Here, $\text{Conv}_{3\times 3}$ and $\text{Conv}_{1\times 1}$ are conv-layers with kernel size 3 and 1, and Avg is global average pooling. The fused features are further concatenated and denoised using a set of dilated 3×3 conv-layers. The output is concatenated to F'_1 and processed by a 3×3 conv-layer to yield the mask prediction.

Our Correlation DINO is optimized end-to-end using cross-entropy loss. It significantly alleviates the overfitting problem in challenging real-world CIML tasks for SDG.

IV. MIMLV2 DATASET

In this section, we introduce MIMLv2, a large-scale, diverse, and high-quality dataset. **The key idea is to leverage constrained image manipulation localization models trained on existing datasets to automatically annotate manually forged images collected from the web.** To ensure high annotation quality, we propose a novel metric that filters out inadequate annotations.

Our MIMLv2 is annotated using our CAAAv2, which is significantly more accurate than its conference version,

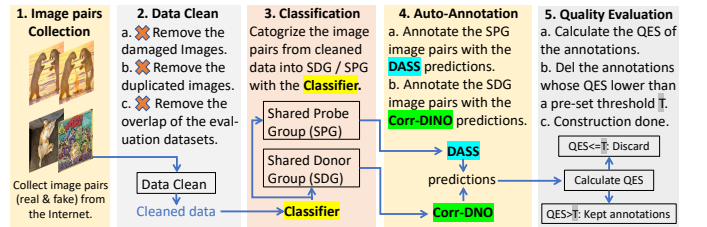


Fig. 7. The overall construction pipeline of our MIMLv2 dataset.

CAAA [14]. As a result, more samples are retained as high quality after filtering, as shown in Table I. Compared to MIMLv1 [14], MIMLv2 offers greater scale and diversity, making it a more effective resource for training IML models.

A. Dataset Construction

As illustrated in Fig. 7, we construct MIMLv2 through the following steps:

Image Collection. We collect forged images and their corresponding originals from imgur.com. On this website, the images are manually manipulated and thus have high-quality, diverse forged regions. Additionally, we exclude images that already appear in the evaluation datasets (Section VII) and remove duplicates by checking their MD5 and pHash.

Auto-Annotation. We utilize the CAAAv2 models, as proposed in Section III, to obtain mask annotations for the collected images. These models are sufficiently trained with one million synthetic COCO samples [26], along with the handcrafted datasets CASIAv2 [31] and IMD20 [32].

Quality Evaluation. After auto-annotation, SPG annotations are already high-quality, whereas a subset of SDG annotations remain unsatisfactory. To ensure overall quality, we propose a novel metric, the Quality Evaluation Score (QES), to further filter unreliable annotations. **The key idea behind QES is to assess the confidence and edge sharpness of predictions, and subsequently remove inadequate predictions.** Specifically, given a prediction mask with shape (H, W)

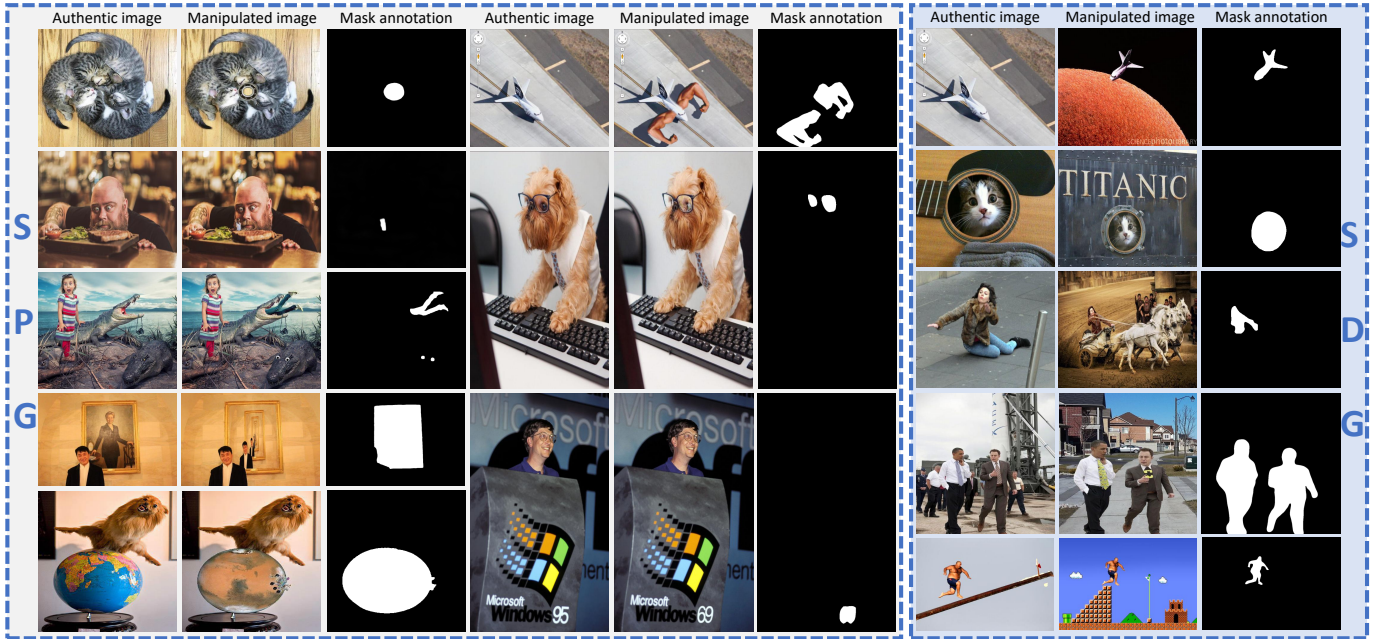


Fig. 8. Some images and their corresponding mask annotations from the proposed MIMLv2 dataset. Left: SPG image pairs. Right: SDG image pairs.

and normalized probability, we compute the QES as follows:
$$QES = \frac{\sum_{i,j}^{H,W} p_{i,j} > (1-T_h)}{\sum_{i,j}^{H,W} p_{i,j} > T_l}$$
, where $\sum_{i,j}^{H,W} p_{i,j} > (1-T_h)$ denotes the area of prediction with a high confidence greater than $(1 - T_h)$, and $\sum_{i,j}^{H,W} p_{i,j} > T_l$ denotes the total predicted potentially manipulated area. We empirically set T_h and T_l to $\frac{1}{16}$ and only retain samples with $QES > 0.5$. Experiments demonstrate that QES can effectively filter unreliable mask annotations, yielding high-quality results.

B. Dataset Highlights

We present a few samples of the proposed MIMLv2 dataset in Fig. 8. The main highlights of our dataset are as follows:

- **High quality.** Image manipulations in the proposed dataset are meticulously crafted by humans. Such data can teach models to detect real-world forgery, rather than merely overfitting to simple patterns found in synthetic data.
- **Large Scale.** As shown in Table I, the proposed dataset comprises 246,212 manually forged images. This is dozens of times more samples than previous handcrafted IML datasets (e.g., ≈ 120 times more samples than IMD20 [32]).
- **Board Diversity.** MIMLv2 comprises images of various sizes, styles, and manipulation types (e.g., copy-move, splicing, removal, AIGC). These images are created by hundreds of thousands of individuals using various software. Such broad diversity can considerably enhance the generalization ability of deep IML models.
- **Modern Style.** MIMLv2 contains abundant modern images that were recently captured and forged, reflecting current photography and forgery technologies. In contrast, the CASIA dataset [31] proposed over a decade ago, features blurred small images and outdated forgeries. Therefore, MIMLv2 better meets the current requirements for IML.
- **Strong Scalability.** With the rising popularity of online image manipulation competitions (e.g., PS-Battles [33], which attracts over 20 million participants), new manually forged

TABLE I
COMPARISON BETWEEN DIFFERENT HANDCRAFTED IMAGE MANIPULATION LOCALIZATION DATASETS. 'NUM.' DENOTES NUMBER.

Name	Year	Real Num.	Forged Num.	(Height, Width) Range
CASIAv1 [31]	2013	800	921	(246, 384)-(500, 334)
CASIAv2 [31]	2013	7461	5,123	(160, 240)-(901, 600)
Coverage [34]	2016	100	100	(190, 334)-(472, 752)
NIST16 [35]	2016	224	564	(500, 500)-(3744, 5616)
In Wild [36]	2018	0	201	(650, 650)-(2736, 3648)
IMD20 [32]	2020	414	2,010	(193, 260)-(4437, 2958)
MIMLv1 [14]	2024	0	123,150	(45, 120)-(13846, 9200)
MIMLv2 (Ours)	2025	63,847	246,212	(45, 120)-(13846, 9200)

images are continuously generated. Our dataset construction approach is ready to harness this growing cheap web data. Therefore, our dataset can be easily expanded in the future.

V. OBJECT JITTER

We experimentally find that the IML model performance can be further improved with more high-quality data. To this end, we introduce Object Jitter, an effective method that enhances IML models by generating high-quality image artifacts online during training from authentic web images.

Previous works synthesize tampered images by randomly cropping and pasting image objects [9], [37]. However, these data synthesis methods often produce overly obvious artifacts and semantically unreasonable content, as shown on the left in Fig. 9. Models trained on such data typically overfit to simple cases and perform poorly on real-world forgeries, where artifacts are subtle and tampered content is semantically reasonable. DEFACTO [8] attempts to ensure semantic reasonableness by designing elaborate rules. It manually identifies eight object types with consistently similar shapes and appearances (e.g., the road sign in the middle of Fig. 9); copy-move or splicing operations are restricted to objects of the same type. Because DEFACTO applies only to a limited number of object classes, the generated data lacks diversity, causing models to overfit the semantics of these specific object types.



Fig. 9. Comparison between different data generation methods. Our method is universally applicable and always produces semantically reasonable forgeries.

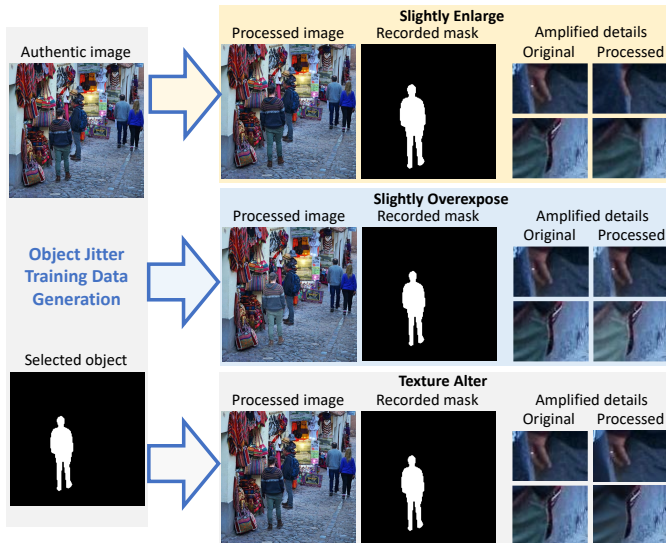


Fig. 10. The proposed Object Jitter method. Given a randomly selected object from an authentic image, we slightly enlarge or overexpose it, or alter its texture. The processed object is regarded as tampered object for training.

Furthermore, DEFACTO heavily relies on accurate object class annotations, which significantly limits its broader application.

To overcome these challenges, we propose a novel idea: **instead of altering image semantics through tampering, we simulate subtle artifacts**. Building on this idea, we introduce Object Jitter, a novel method detailed in Fig 10. Given an input image, we readily obtain a segmentation mask for a random object using off-the-shelf segmentation models like SAM [38]. The selected object is then processed using one or a combination of the following three random operations:

- **Size Jitter**. Slightly enlarge the selected object’s region and its corresponding mask by a random scale.
- **Exposure Jitter**. Slightly overexpose the selected object.
- **Texture Jitter**. Slightly alter the texture of the selected object region by applying a random combination of JPEG compression, reverse JPEG compression [39], and blur.

After processing, we add a random smooth transition on the edges to minimize visual artifacts. We apply Object Jitter to 1 to 3 random objects within an input image. The mask regions of these processed objects are recorded and subsequently considered as tampered regions during training.

Our method successfully addresses existing issues: **First**, it always preserves the semantics of the input image, thereby preventing models from overfitting to simple cases with abnormal semantics. **Second**, by applying subtle changes to objects that already naturally blend into the background, the generated visual image artifacts are unobvious. **Third**, our method is unconstrained and universally applicable. Consequently, Object Jitter consistently produces high-quality artifacts and effectively supplements our MIMLv2 dataset.

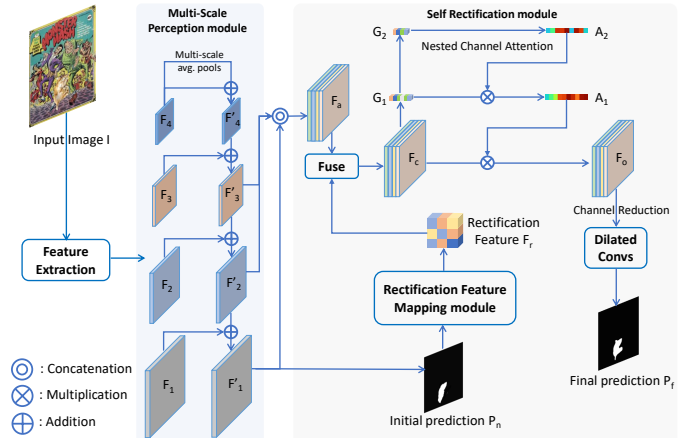


Fig. 11. The overall framework of the proposed Web-IML model.

VI. WEB-IML

To better leverage the web-scale supervision, we propose a new model called Web-IML. As illustrated in Fig. 11, Web-IML comprises a feature extractor, a Multi-Scale Perception module to integrate information from multiple perspectives, and a Self-Rectification module that enables the model to identify and correct its mistakes.

Multi-Scale Perception module motivation. During meticulous image forensic analysis, humans often zoom in and out the image repeatedly, comparing between diverse observations to assist their final prediction. To mimic the human perception way, we introduce the Multi-Scale Perception module.

Multi-Scale Perception module pipeline. Specifically, given four feature maps extracted from the backbone model F_1, F_2, F_3, F_4 , we first extract global features in different scales: $G_i = Conv_{1 \times 1}(Avg_i(F_4))$ for $i \in \{1, 2, 3, 6\}$, where $Conv_{1 \times 1}$ denotes conv-layer with kernel size 1 and Avg_i denotes average pooling function with output size $i \times i$. The global features are then resized, concatenated to F_4 and fused, dimension reduced to get F'^4 . $F'^4 = Conv_{3 \times 3}([G_1, G_2, G_3, G_6, F_4])$. Next, the high-level features are fused with the low-level features recursively. $F'_n = Conv_{3 \times 3}(F'_{n+1} + Conv_{1 \times 1}(F_n))$ for $i \in \{1, 2, 3\}$. This process fully integrates high-level semantics with low-level image details, resulting in the multi-scale features F'_1, F'_2, F'_3, F'_4 .

Self-Rectification module motivation. Due to the challenging nature of the image manipulation localization task, forensic models inevitably overlook key information and make mistakes. To minimize negligence, we propose the Self-Rectification module. With this module, our model can learn to check and correct its initial predictions.

Self-Rectification module pipeline. As shown at the bottom of Fig. 11, we obtain the initial mask prediction P_n from F'_1 via a 1×1 conv-layer. We then adaptively obtain a rectification feature F_r through a tiny Rectification Feature

TABLE II

COMPARISON ON IMAGE MANIPULATION LOCALIZATION. "WS" IS OUR PROPOSED WEB SUPERVISION, WHICH TRAINS MODELS USING DATA FROM THE MIMLV2 AND OBJECT JITTER. "AVG*" IS THE AVERAGE SCORE EXCLUDING IMD20. "PARAM." IS THE NUMBER OF MODEL PARAMETERS.

Method	CASIaV1 [31]		Coverage [34]		NIST16 [35]		IMD20 [32]		CocoGlide [10]		CIMD [40]		MISD [41]		Avg.*		Average		Param.
	IoU	F1	IoU	F1	IoU	F1	IoU	F1	IoU	F1	IoU	F1	IoU	F1	IoU	F1	IoU	F1	
ManTra-Net [42]	.086	.130	.181	.271	.040	.062	.098	.146	.155	.203	.058	.096	.105	.171	.104	.156	.103	.154	8M
Rru-Net [43]	.330	.380	.165	.260	.080	.129	.169	.256	.223	.304	.036	.068	.440	.570	.212	.285	.206	.281	5M
MVSS-Net [20]	.403	.435	.389	.454	.243	.294	.200	.260	.276	.357	.016	.021	.120	.175	.235	.284	.235	.285	146M
PSCC-Net [37]	.410	.463	.340	.446	.067	.110	.115	.192	.333	.422	.212	.290	.400	.491	.294	.370	.268	.345	4M
CAT-Net [7]	.684	.738	.238	.292	.238	.302	-	-	.290	.366	.282	.344	.314	.394	.341	.406	-	-	114M
IF-OSN [28]	.465	.509	.181	.268	.247	.326	.259	.364	.207	.264	.195	.295	.375	.464	.278	.354	.341	.406	124M
EVP [44]	.438	.502	.078	.114	.188	.239	.177	.268	.084	.118	.224	.283	.392	.531	.234	.298	.276	.356	63M
TruFor [10]	.630	.692	.446	.522	.279	.348	-	-	.294	.362	.322	.418	.426	.549	.400	.482	-	-	67M
PIM [25]	.512	.566	.188	.251	.225	.280	.340	.419	.327	.404	.177	.229	.389	.519	.303	.375	.308	.381	168M
APSC-Net [14] (Conf.)	.799	.837	.490	.523	.398	.436	.339	.391	.243	.283	.517	.565	.420	.524	.477	.528	.458	.508	143M
Web-IML (Ours)	.823	.857	.508	.551	.412	.465	.370	.422	.285	.339	.629	.673	.430	.545	.515	.572	.494	.550	140M
APSC-Net (w/ MIMLV1)	.810	.848	.498	.568	.525	.590	.679	.760	.292	.355	.652	.720	.484	.587	.543	.611	.562	.632	143M
Web-IML (w/ MIMLV1)	.821	.854	.561	.616	.520	.587	.692	.768	.275	.325	.789	.845	.496	.610	.578	.640	.594	.658	140M
APSC-Net (w/ WS)	.832	.865	.594	.642	.578	.661	.690	.766	.389	.451	.660	.725	.485	.588	.598	.655	.604	.671	143M
Web-IML (w/ WS)	.846	.879	.715	.768	.591	.670	.698	.776	.439	.507	.759	.821	.495	.612	.641	.709	.649	.719	140M

TABLE III

ABLATION STUDY ON OUR WEB-IML MODEL. 'MP' IS THE MULTI-SCALE PERCEPTION MODULE. 'SR' IS THE SELF-RECTIFICATION MODULE. 'NA' IS OUR NESTED CHANNEL ATTENTION. 'RF' DENOTES THE SECOND ROUND SELF-RECTIFICATION. 'WS' DENOTES THE PROPOSED WEB SUPERVISION.

Num.	Ablation Settings					CASIaV1 [31]		Coverage [34]		NIST16 [35]		IMD20 [32]		CocoGlide [10]		CIMD [40]		MISD [41]		Average	
	MP	SR	NA	RF	WS	IoU	F1	IoU	F1	IoU	F1	IoU	F1	IoU	F1	IoU	F1	IoU	F1	IoU	F1
(1)	×	×	×	×	×	.711	.779	.361	.430	.346	.410	.273	.342	.345	.417	.262	.338	.362	.471	.380	.455
(2)	✓	×	×	×	×	.775	.814	.440	.487	.359	.415	.351	.406	.275	.324	.450	.502	.375	.482	.432	.490
(3)	✓	✓	×	×	×	.802	.836	.523	.576	.385	.441	.364	.415	.287	.343	.557	.610	.382	.493	.471	.530
(4)	✓	✓	✓	×	×	.816	.848	.549	.598	.394	.449	.369	.419	.291	.345	.593	.649	.386	.496	.486	.543
(5)	✓	✓	✓	✓	×	.823	.857	.508	.551	.412	.465	.370	.422	.285	.339	.629	.673	.430	.545	.494	.550
(6)	✓	✓	✓	✓	✓	.846	.879	.715	.768	.591	.670	.698	.776	.439	.507	.759	.821	.496	.612	.649	.719

TABLE IV

ROBUSTNESS EVALUATION WITH AUC METRIC ON NIST16 DATASET.

Method	Ori	Resize		Blur		JPEG	
		.78x	.25x	k=3	k=15	q=100	q=50
ManTra-Net [42]	.795	.774	.755	.774	.746	.779	.744
SPAN [45]	.840	.832	.802	.831	.792	.836	.807
PSCC-Net [37]	.855	.853	.850	.854	.800	.854	.854
ObjectFormer [22]	.872	.872	.863	.860	.803	.864	.862
Sparse ViT [6]	.888	.884	.869	.881	.877	.886	.881
ERMPC [46]	.895	.893	.877	.892	.871	.894	.888
UnionFormer [47]	.881	.873	.872	.865	.843	.880	.880
APSC-Net+MIMLV1	.928	.917	.888	.907	.900	.922	.907
Web-IML (Ours)	.942	.935	.904	.914	.900	.940	.909

Mapping module (RFM), which consists of 5 cascaded conv-layers. $F_r = RFM(P_n)$. The F_r informs the model of suspected tampered regions and potentially incorrect prediction regions. Then F_r is fused with F_a with a 3×3 conv-layer to get F_c . $F_c = Conv_{3 \times 3}([F_a, P_c])$. To enable in-depth, meticulously analyses of F_c , we introduce the Nested Channel Attention module. As shown in the top left of Fig. 11, it can be formulated as $G_1 = Avg(F_c)W_1$, $G_2 = G_1W_2$, $A_2 = \sigma(W_3G_2)$, $A_1 = \sigma(W_4G_1 * A_2)$, $F_o = F_c * A_1$. Here, $G_{1,2}$ are global vectors, $A_{1,2}$ are attention maps, $W_{1,2,3,4}$ are learnable parameters, Avg is global average pooling and σ is the sigmoid function. The output F_o is further processed by four 3×3 conv-layers with dilation sizes 1, 2, 3, 6 respectively, the output features are concatenated and fused with a 3×3 conv-layers. The mask prediction P_f is obtained from F_o with a 1×1 conv-layer. To get the refined final prediction P_f , we replace P_n with P_f , replace F_a with F_o , then repeat the self rectification once again.

Our Web-IML is optimized with the cross entropy loss calculated between the prediction mask and the ground-truth.

VII. EXPERIMENTS

A. Experiments on the Web-IML Model (IML Task)

This subsection evaluates the effectiveness of the proposed Web-IML model by comparing it with other IML models on multiple real-world handcrafted and AIGC forgery benchmarks. We also perform an ablation study to provide an in-depth analysis of the Web-IML model.

Implementation Details. For Web-IML, we adopt ConvNeXt-Base [50] as the feature extractor. The model is trained for 200k iterations with a batch size of 16, using a 512×512 input size, consistent with previous works [7], [10]. We employ Cross-Entropy loss and AdamW [14] optimizer, with the learning rate linearly decaying from $1e-4$ to $1e-6$. CASIAv2 [31] and tampCOCO [7] serve as baseline training sets. For fair comparison, mask predictions are binarized with a fixed threshold of 0.5 and evaluated using IoU and binary F1-score. **Comparison Study.** Table II shows that our Web-IML significantly outperforms existing methods on multiple real-world image forgery benchmarks. For example, it achieves an average IoU that is 24.1 points higher than TruFor. *Furthermore, Web-IML consistently outperforms our conference version, APSC-Net, across various settings.* These results demonstrate the strong generalization capabilities of our Web-IML model. Qualitative comparison is illustrated in Fig. 12.

Ablation Study. The ablation results are shown in Table III. Setting (2), which includes the proposed Multi-Scale Perception (MP) module, achieves 5.2 points higher IoU than the baseline (1). This indicates that the proposed MP module effectively integrates high-level and low-level features to detect diverse image artifacts. Setting (3), which further incorporates the Self-Rectification (SR) module, yields an additional 3.9

TABLE V

ABLATION STUDY ON OUR WEB SUPERVISION METHOD WITH WEB-IML MODEL. ‘PSCC-SYNTHETIC’ DENOTES THE SYNTHETIC DATA FROM THE PSCC-NET [37]. ‘O.J.’ DENOTES THE PROPOSED OBJECT JITTER METHOD. ‘C.G.’ DENOTES THE COCOGLIDE [10]. ‘Δ’ DENOTES IMPROVEMENT.

Num.	Training Data	CASIv1 [31]		Coverage [34]		NIST16 [35]		IMD20 [32]		C.G. [10]		CIMD [40]		MISD [41]		Average (#Δ)	
		IoU	F1	IoU	F1	IoU	F1	IoU	F1	IoU	F1	IoU	F1	IoU	F1	IoU	F1
(1)	Baseline	.823	.857	.508	.551	.412	.465	.370	.422	.285	.339	.629	.673	.430	.545	.494 (+0.0%)	.550 (+0.0%)
(2)	+PSCC-Synthetic [37]	.813	.845	.503	.546	.348	.392	.361	.410	.177	.211	.598	.654	.330	.441	.447 (-9.5%)	.500 (-9.1%)
(3)	+DEFACTO [8]	.809	.843	.354	.380	.412	.465	.365	.424	.359	.418	.394	.438	.461	.572	.451 (-8.7%)	.506 (-8.0%)
(4)	+AIGC-Synthetic [48]	.817	.849	.273	.296	.220	.276	.284	.337	.394	.462	.287	.340	.373	.429	.376 (-24.%)	.420 (-23.%)
(5)	+MIMLv1 [14] (<i>Conf.</i>)	.821	.854	.561	.616	.520	.587	.692	.768	.275	.325	.789	.845	.496	.610	.594 (+20.%)	.658 (+20.%)
(6)	+MIMLv2	.849	.883	.694	.755	.518	.584	.697	.772	.376	.435	.716	.776	.448	.564	.614 (+24.%)	.681 (+24.%)
(7)	+MIMLv1 [14]+O.J.	.833	.867	.587	.643	.549	.620	.693	.768	.344	.407	.793	.849	.487	.602	.612 (+24.%)	.679 (+23.%)
(8)	+O.J.	.822	.853	.575	.616	.270	.310	.422	.482	.308	.362	.698	.760	.413	.521	.501 (+1.4%)	.558 (+1.4%)
(9)	+MIMLv2+O.J. (Ours)	.846	.879	.715	.768	.591	.670	.698	.776	.439	.507	.759	.821	.496	.612	.649 (+31.%)	.719 (+31.%)

TABLE VI

ABLATION STUDY ON OUR OBJECT JITTER METHOD. ‘COCO’ DENOTES USING THE COCO [49] DATASET IMAGES FOR OBJECT JITTER. ‘SA’ DENOTES USING 400K RANDOM IMAGES FROM THE SA-1B [38] DATASET FOR OBJECT JITTER. ‘C.G.’ DENOTES THE COCOGLIDE DATASET [10].

Num	Object Jitter Operation			Image Source	CASIv1 [31]		Coverage [34]		NIST16 [35]		IMD20 [32]		C.G. [10]		CIMD [40]		MIFD [41]		Average	
	Size	Texture	Exposure		IoU	F1	IoU	F1	IoU	F1	IoU	F1	IoU	F1	IoU	F1	IoU	F1	IoU	F1
(1)	×	×	×	SA	.849	.883	.694	.755	.518	.584	.697	.772	.376	.435	.716	.776	.448	.564	.614	.681
(2)	×	✓	✓	SA	.839	.872	.634	.687	.528	.592	.703	.778	.396	.456	.748	.798	.487	.605	.619	.684
(3)	✓	×	✓	SA	.844	.878	.669	.729	.554	.618	.701	.778	.427	.491	.780	.834	.501	.616	.640	.706
(4)	✓	✓	×	SA	.839	.872	.699	.754	.560	.627	.699	.774	.413	.479	.802	.861	.512	.628	.646	.714
(5)	✓	×	×	SA	.841	.875	.673	.732	.540	.602	.701	.777	.432	.496	.758	.816	.516	.631	.637	.704
(6)	✓	✓	✓	COCO	.848	.881	.645	.711	.584	.657	.699	.776	.489	.549	.803	.864	.496	.612	.652	.721
(7)	✓	✓	✓	SA	.846	.879	.715	.768	.591	.670	.698	.776	.439	.507	.759	.821	.496	.613	.649	.719

point IoU improvement over Setting (2), as SR enables the model to detect and correct its errors. Setting (5) outperforms (4) via our nested attention module that enables in-depth analysis. Setting (6) outperforms (5) by including a second round of self-rectification refinement, demonstrating that further refinement can minimize incorrect predictions.

Robustness Evaluation. We evaluate Web-IML under various distortions, including image resizing (scale factors 0.78 and 0.25), Gaussian blur (kernel sizes 3 and 15), and JPEG compression (quality factors 50 and 100). The results are shown in Table IV. Our model exhibits stable performance under these conditions, demonstrating strong robustness.

B. Experiments on the Web-Supervision Method (IML Task)

This subsection evaluates the effectiveness of our proposed web-supervision approach in addressing the data scarcity issue for IML. Our web-supervision encompasses both the MIMLv2 dataset and the Object Jitter method. We compare the performance of the same IML model trained on data created by our web-supervision approach against other synthetic methods.

Implementation Details. The implementation details remain the same as in the previous subsection VII.A. When supplementing the baseline training sets with additional IML training sets, the total training volume is kept constant with a uniform sampling ratio across all datasets.

Comparison Study for the MIMLv2 Dataset. Table V presents the IML performance of the Web-IML model when trained on different datasets. The baseline (1) uses the two commonest training sets: tampCOCO [7] and CASIAv2 [31]. Incorporating synthetic training data from PSCC-Net [37], DEFACTO [8] or OpenSDID [48] diminishes the average model performance (settings 2, 3, 4). This is because the first two synthetic datasets do not notably surpass the baseline data in quality or diversity, while the AIGC forgeries from OpenSDID differ significantly from non-AIGC forgeries. These results

confirm that merely increasing training data scale does not lead to improved performance. In contrast, including the MIMLv1 (setting 5) or MIMLv2 (setting 6) datasets significantly improves model performance by an average of 10 and 12 points, respectively, without increasing training or inference burden. These results confirm that our MIMLv1 and MIMLv2 datasets considerably alleviate data scarcity and overfitting issues in real-world scenarios. This is attributable to their large scale, manual forgery, and considerably higher quality and diversity compared to other datasets. *Notably, MIMLv2 yields greater improvement due to its larger quantity of high-quality samples and superior diversity compared to MIMLv1.*

Comparison Study for the Object Jitter. Table V shows that including the training data generated by our Object Jitter method further improves the model when combined with MIMLv1 (setting 7 outperforms 5) or MIMLv2 (setting 9 outperforms 6) datasets, effectively supplementing them. This is attributed to our Object Jitter method’s consistent generation of diverse, high-quality samples, which further enriches the training data.

Ablation Study for the Object Jitter. Table VI presents the ablation study for Object Jitter operations and image source. Setting (1) is the baseline, where Web-IML is trained with MIMLv2 but without Object Jitter. Setting (7) represents the full Object Jitter method. Settings (2, 3, 4) involve removing the size jitter, texture jitter, and exposure jitter operations, respectively; all of them result in worse performance than setting (7). These results demonstrate that all three operations contribute to improved performance through increased data diversity. Notably, Setting (2), which lacks size jitter, is significantly worse than (7). Meanwhile, Setting (5), which uses only size jitter, performs close to (7). This indicates that the size jitter operation is the primary contributor to the improvement. Since most Internet forgeries are not generated by copy-move, they exhibit exposure and texture artifacts. The size jitter operation, without altering the object’s exposure or

TABLE VII

COMPARISON STUDY OF OUR WEB-SUPERVISION ON IML TASK. **BLUE NUMBER FOR IMPROVEMENT** AND **RED NUMBER FOR DECREASE**. 'B.L.' DENOTES BASELINE SETTING USING TAMP-COCO [7] AND CASIAV2 [31] DATASETS AS TRAINING DATA. 'PSCC-SYNTH.' DENOTES THE SYNTHETIC DATASET OF PSCC-NET [37], 'AIGC-SYNTH.' DENOTES THE AIGC FORGERY DATASET OPENSDDID [48]. 'O.J.' DENOTES OUR OBJECT JITTER METHOD.

Training Data	CASIAv1 [31]				Coverage [34]				NIST16 [35]				IMD20 [32]				CIMD [40]				Average			
	IoU	Δ	F1	Δ	IoU	Δ	F1	Δ	IoU	Δ	F1	Δ	IoU	Δ	F1	Δ	IoU	Δ	F1	Δ	IoU	Δ	F1	Δ
PSCC-Net B.L.	.401	0	.430	0	.197	0	.218	0	.247	0	.295	0	.125	0	.156	0	.161	0	.221	0	.226	0	.264	0
+PSCC-Synth.	.352	12%	.379	12%	.147	25%	.159	27%	.230	7%	.274	7%	.101	19%	.125	20%	.101	37%	.124	44%	.186	18%	.212	20%
+DEFACTO [8]	.394	2%	.429	1%	.231	17%	.256	17%	.223	10%	.270	8%	.157	26%	.171	10%	.120	25%	.159	28%	.225	0%	.257	3%
+AIGC-Synth.	.346	16%	.377	14%	.109	81%	.123	77%	.091	171%	.142	108%	.110	14%	.144	8%	.124	30%	.170	30%	.156	45%	.191	38%
+MIMLv1 (Conf.)	.609	52%	.649	51%	.395	101%	.477	119%	.402	63%	.476	61%	.470	276%	.541	247%	.206	28%	.251	14%	.416	84%	.479	81%
+MIMLv2	.602	50%	.642	49%	.402	104%	.498	128%	.405	64%	.485	64%	.575	360%	.662	324%	.354	120%	.483	119%	.468	+107%	.554	110%
+MIMLv2+O.J.	.609	52%	.651	51%	.451	129%	.550	152%	.406	64%	.486	65%	.570	356%	.658	322%	.335	108%	.464	110%	.474	110%	.562	113%
CAT-Net B.L.	.660	0	.703	0	.245	0	.286	0	.239	0	.287	0	.157	0	.192	0	.229	0	.263	0	.306	0	.346	0
+PSCC-Synth.	.410	38%	.437	38%	.215	12%	.232	19%	.288	21%	.331	15%	.121	23%	.148	23%	.160	30%	.189	28%	.239	22%	.268	23%
+DEFACTO [8]	.673	2%	.715	2%	.200	18%	.230	20%	.220	8%	.261	9%	.164	4%	.200	4%	.130	43%	.156	41%	.277	9%	.312	10%
+AIGC-Synth.	.646	2%	.685	3%	.136	80%	.147	95%	.170	41%	.242	19%	.130	21%	.165	16%	.088	160%	.117	125%	.234	31%	.271	28%
+MIMLv1 (Conf.)	.691	5%	.728	4%	.302	23%	.389	36%	.353	48%	.422	47%	.547	248%	.629	228%	.397	73%	.477	81%	.458	50%	.529	53%
+MIMLv2	.684	4%	.720	2%	.368	50%	.443	55%	.338	41%	.416	45%	.562	258%	.644	235%	.470	105%	.548	108%	.484	58%	.554	60%
+MIMLv2+O.J.	.703	7%	.742	6%	.355	45%	.437	53%	.358	50%	.440	53%	.575	266%	.656	242%	.497	117%	.575	119%	.498	63%	.570	65%
TruFor B.L.	.755	0	.794	0	.363	0	.411	0	.320	0	.377	0	.248	0	.289	0	.296	0	.346	0	.396	0	.443	0
+PSCC-Synth.	.750	1%	.798	1%	.340	7%	.384	7%	.325	2%	.373	1%	.253	2%	.298	3%	.278	6%	.331	5%	.389	2%	.437	2%
+DEFACTO [8]	.752	0%	.791	0%	.322	13%	.357	15%	.214	50%	.260	45%	.209	19%	.247	17%	.184	61%	.217	59%	.336	18%	.374	18%
+AIGC-Synth.	.746	1%	.791	0%	.220	65%	.261	57%	.213	50%	.263	43%	.221	12%	.267	8%	.121	146%	.156	122%	.304	30%	.348	28%
+MIMLv1 (Conf.)	.755	0%	.794	0%	.385	6%	.458	10%	.352	9%	.408	8%	.596	58%	.678	57%	.340	13%	.401	14%	.486	18%	.548	19%
+MIMLv2	.767	2%	.794	0%	.387	6%	.458	10%	.407	21%	.472	20%	.618	60%	.696	58%	.370	20%	.422	18%	.510	22%	.568	22%
+MIMLv2+O.J.	.770	2%	.811	2%	.466	22%	.511	20%	.439	27%	.502	25%	.619	60%	.700	59%	.309	4%	.357	3%	.521	24%	.576	23%

TABLE VIII

COMPARISON STUDY OF CIML ON SPG (LEFT) AND SDG (RIGHT). '*' DENOTES MODEL TRAINED WITH BOTH SDG AND SPG DATA. 'NONZERO' DENOTES USING THE NON-ZERO REGION OF THE DIFFERENCE MAP AS MASK, 'OTSU' DENOTES THE DIFFERENCE MAP BINARIZED BY OTSU. 'QES' DENOTES THE PREDICTIONS FILTERED BY OUR QES METRIC.

CIML on SPG					CIML on SDG				
Method	P	R	F	IoU	Method	P	R	F	IoU
Nonzero	.159	.987	.273	.079	DMVN* [26]	.553	.357	.434	.276
OSTU [29]	.812	.589	.683	.497	DMVN [26]	.438	.568	.495	.317
DMVN* [26]	.329	.618	.430	.276	DMAC* [51]	.583	.538	.559	.410
DMVN [26]	.682	.781	.728	.578	DMAC [51]	.703	.622	.660	.518
DMAC* [51]	.617	.624	.620	.432	SACM [14] (Conf.)	.778	.819	.798	.702
DMAC [51]	.746	.710	.728	.573	Corr-DINO (Ours)	.816	.862	.838	.744
DASS (Ours)	.860	.921	.889	.835	Corr-DINO (QES)	.939	.971	.954	.912

texture, reduces model's reliance on exposure or texture cues, thus better supplementing MIMLv2. Furthermore, Setting (6) applies the full Object Jitter method using COCO [49] as the image source, instead of 400k random images from SA [38] in setting (7). The similar performance of Settings (6) and (7) demonstrates that the Object Jitter method is robust to the choice of image source.

Conclusions Verification on Other IML Models. We extended our verification process to other IML models. Specifically, we evaluated MIMLv2 and Object Jitter on PSCC-Net [37], CAT-Net [7], and TruFor [10] using their official model code. Table VII presents the results, which clearly indicate that MIMLv1, MIMLv2, and Object Jitter all lead to significantly higher scores. *MIMLv2, in particular, consistently yields significantly greater improvement than MIMLv1 (conference version).* Moreover, *Object Jitter further boosts performance when integrated with MIMLv2.* These results robustly confirm our previous analyses and conclusions.

C. Experiments on the CAAAv2 Models (CIML task)

This subsection evaluates the effectiveness of the proposed CAAAv2 in the CIML task by comparing its DASS and Corr-DINO models against other CIML models on SPG and SDG

TABLE IX

ABLATION STUDY OF CIML ON SPG. 'FORGED' DENOTES USING THE FORGED IMAGE AS INPUT, 'AUTH.' DENOTES USING THE AUTHENTIC IMAGE AS INPUT, 'DIFF.' DENOTES USING THE ABSOLUTE DIFFERENCE MAP BETWEEN THE FORGED AND AUTHENTIC IMAGE AS INPUT.

Num.	Backbone	Forged	Auth.	Diff.	P	R	F1	IoU
(1)	VGG [52]	✓	×	×	.423	.365	.392	.236
(2)	VGG [52]	✓	✓	×	.800	.857	.827	.718
(3)	VGG [52]	×	×	✓	.771	.857	.812	.741
(4)	VGG [52]	✓	✓	✓	.825	.899	.860	.781
(5)	VAN [30]	✓	×	×	.573	.533	.552	.408
(6)	VAN [30]	✓	✓	✓	.860	.921	.889	.835

test datasets, respectively. We also conduct detailed ablation studies for in-depth analysis.

Implementation Details. Given that real-world forgeries in the IMD20 [32] dataset closely resemble the target images for annotation, we use a portion of this dataset to evaluate model performance using IoU and binary F1-score metrics. We categorize the forged images in IMD20 into SPG or SDG and randomly split them into training and test sets with a 3:1 ratio. CASIAv2 [31] and approximately 1M images synthesized from the COCO [49] dataset are also used for training. Input images are resized to 512×512, and a consistent training pipeline is applied across all methods.

Comparison Study. Table VIII presents comparison results for SPG (left) and SDG (right) separately. Our method clearly outperforms these previous methods, primarily because our category-aware paradigm significantly reduces task difficulty. As shown in the right side of Table VIII, our Corr-DINO, prior to QES filtering, achieves an IoU of 0.744. *This is 4.2 points higher than the SACM [14] (our conference version),* demonstrating that our frozen-denoising paradigm notably alleviates the overfitting issue when training on limited data. Notably, DMVN [26] and DMAC [51] models trained on both SPG and SDG data perform worse than those trained exclusively on one category. This is attributed to the confusion caused by similar backgrounds in SPG image pairs.

Ablation Study for the DASS Model Input. Table IX

presents the results, confirming that both the image pair and the image difference map are essential for accurate prediction in SPG. The image difference map between forged and authentic images can roughly indicate the forged regions, while the images themselves provide semantic information to help the model denoise the difference map.

Ablation Study for the Corr-DINO Model Backbone. The results are shown in Table X, settings (1-19). For the ConvNeXt CNN model, the trainable version performs better. For all ViT models, however, frozen versions perform significantly better. Since ViT models tend to overfit with limited training data, freezing the backbone alleviates catastrophic forgetting and overfitting. LoRA [53] fine-tuned versions exhibit similar performance to their frozen counterparts, as LoRA also mitigates forgetting. The frozen DINOv2-Base [13] backbone performs optimally and is therefore adopted.

Ablation Study of the Corr-DINO Model Modules. The results are shown in the bottom of Table X, setting (20) is the baseline without any proposed modules, setting (24) is the full model with all proposed modules. In settings (21, 22, 23), we remove the proposed Multi-Aspect Denoiser, Feature Super Resolution and Learnable Aggregation modules from the full model (24) respectively. Setting (24) significantly outperforms (21). This validates that correlation features extracted from the frozen DINOv2 are highly noisy, and that denoising through multi-aspect feature integration is essential for accurate predictions. Setting (24) also significantly outperforms (22). This confirms that initial correlation features are too coarse for precise mask predictions, and our Feature Super Resolution module effectively addresses this by reconstructing fine-grained details. Finally, Setting (24) is superior to (23) because our learnable aggregation mitigates information loss inherent in rule-based aggregation.

Ablation Study of the QES. The last two rows of Table X show the results. The results of setting (25) are obtained by evaluating only the predictions from setting (24) where $QES > 0.5$. QES-filtered predictions from setting (25) achieve an IoU of 0.912, representing a 16.8 point increase over setting (24). This confirms that QES effectively filters out unsatisfactory predictions, thereby notably improving annotation quality. Table XI confirms QES’s high relevance to the IoU metric without relying on ground truth for evaluation.

Our Models are Adequate Auto-Annotators. In Table VIII, both our DASS and Corr-DINO achieve high IoU scores. Considering the errors in IMD20’s ground truth [54], especially in SPG images, our actual accuracy is higher. Clearly, our methods are sufficient for obtaining accurate auto-annotations.

D. Experiments on the Downstream Document IML Task

This subsection evaluates the generalization of the Web-IML model and the universal applicability of our web-supervision method on an important downstream task: document IML.

We fine-tune our Web-IML under various pretraining settings on the handcrafted document IML benchmark SACP [58], using the same training and test configurations as prior works [63]. Our Web-IML notably outperforms prior methods. Moreover, Table XII shows that settings (11, 12, 13), which incorporate additional training data from DEFAC²O [8],

TABLE X
ABLATION STUDY OF CIML ON SDG. ‘FREEZE’ DENOTES FREEZING THE BACKBONE AND ‘L’ DENOTES LoRA [53] FINE-TUNING. ‘MAD’ DENOTES THE MULTI-ASPECT DENOISER. ‘FSR’ DENOTES THE FEATURE SUPER RESOLUTION. ‘LA’ DENOTES THE LEARNABLE AGGREGATION. ‘QES’ DENOTES FILTERING THE PREDICTION WITH OUR QES.

Num.	Backbone	Freeze	MAD	FSR	LA	QES	P	R	F1	IoU
(1)	ConvNeXt-B [50]	×	✓	✓	✓	×	.740	.690	.714	.595
(2)	ConvNeXt-B [50]	✓	✓	✓	✓	×	.635	.554	.592	.414
(3)	Eff.SAM [55]	×	✓	✓	✓	×	.483	.624	.544	.381
(4)	Eff.SAM [55]	✓	✓	✓	✓	×	.606	.502	.549	.403
(5)	CLIP-L [56]	×	✓	✓	✓	×	.665	.509	.577	.453
(6)	CLIP-L [56]	L	✓	✓	✓	×	.744	.736	.740	.587
(7)	CLIP-L [56]	✓	✓	✓	✓	×	.749	.721	.735	.596
(8)	DINOv1-B [57]	×	✓	✓	✓	×	.693	.512	.589	.456
(9)	DINOv1-B [57]	L	✓	✓	✓	×	.693	.742	.717	.595
(10)	DINOv1-B [57]	✓	✓	✓	✓	×	.700	.700	.700	.586
(11)	DINOv2-S [13]	×	✓	✓	✓	×	.739	.653	.693	.584
(12)	DINOv2-S [13]	L	✓	✓	✓	×	.783	.733	.758	.637
(13)	DINOv2-S [13]	✓	✓	✓	✓	×	.777	.781	.772	.667
(14)	DINOv2-B [13]	×	✓	✓	✓	×	.705	.574	.633	.472
(15)	DINOv2-B [13]	L	✓	✓	✓	×	.794	.861	.826	.727
(16)	DINOv2-B [13]	✓	✓	✓	✓	×	.816	.862	.838	.744
(17)	DINOv2-L [13]	×	✓	✓	✓	×	.667	.517	.582	.454
(18)	DINOv2-L [13]	L	✓	✓	✓	×	.803	.843	.823	.725
(19)	DINOv2-L [13]	✓	✓	✓	✓	×	.809	.850	.829	.732
(20)	DINOv2-B [13]	✓	×	×	×	×	.644	.605	.624	.469
(21)	DINOv2-B [13]	✓	×	✓	✓	×	.699	.666	.682	.526
(22)	DINOv2-B [13]	✓	✓	×	✓	×	.822	.728	.772	.664
(23)	DINOv2-B [13]	✓	✓	✓	×	×	.804	.838	.821	.719
(24)	DINOv2-B [13]	✓	✓	✓	✓	×	.816	.862	.838	.744
(25)	DINOv2-B [13]	✓	✓	✓	✓	✓	.939	.971	.954	.912

TABLE XI
ABLATION STUDY ON THE THRESHOLD OF QES.

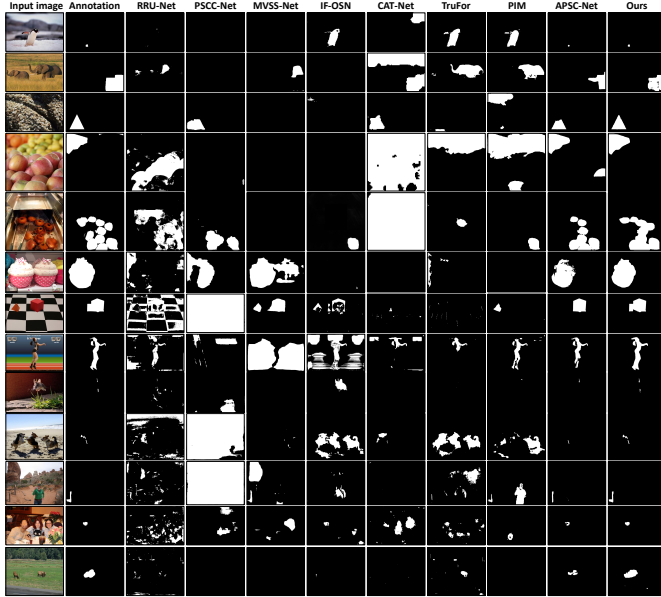
QES Threshold	0.0	0.1	0.2	0.3	0.4	0.5	0.6	0.7	0.8	0.9
kept sample ratio	2.45	1.90	1.84	1.72	1.51	1.00	0.73	0.50	0.31	0.06
IMD20 SDG IoU	.744	.825	.842	.865	.889	.912	.924	.957	.967	.968

TABLE XII
IMAGE MANIPULATION LOCALIZATION PERFORMANCE ON SACP [58] DATASET. ‘FORGERY BASELINE’ DENOTES USING THE TAMPCOCO [7] AND CASIAV2 [31] DATASETS FOR MODEL PRETRAINING

Num.	Methods	Pretraining data	IoU	F1
(1)	DFCN [59]	Image-Net [60]	.466	.607
(2)	MVSS-Net [20]	Image-Net [60]	.401	.534
(3)	PSCC-Net [37]	Image-Net [60]	.482	.620
(4)	RRU-Net [43]	Image-Net [60]	.517	.651
(5)	CFL-Net [61]	Image-Net [60]	.433	.571
(6)	DTD [62]	Image-Net [60]	.588	.712
(7)	TIFDM [63]	Image-Net [60]	.576	.703
(8)	Web-IML (Ours)	Image-Net [60]	.773	.862
(9)	Web-IML (Ours)	ADE20k [64]	.774	.863
(10)	Web-IML (Ours)	Forgery Baseline	.778	.865
(11)	Web-IML (Ours)	(10) + DEFAC ² O [8]	.767	.856
(12)	Web-IML (Ours)	(10) + PSCC Synthetic [37]	.762	.853
(13)	Web-IML (Ours)	(10) + AIGC Synthetic [48]	.756	.851
(14)	Web-IML (Ours)	(10) + MIMLv1 [14] (<i>Conference</i>)	.792	.872
(15)	Web-IML (Ours)	(10) + Web Supervision (Ours)	.800	.880

PSCC [37], and OpenSDID [48] into the baseline (Setting 10), perform worse than the baseline. This confirms that simply increasing the scale and diversity of pretraining data does not lead to better generalization. In contrast, the model pretrained on our web supervision data (15) shows a significant 2.2 point IoU improvement over the baseline (10), and is 0.8 points higher than the model pretrained on MIMLv1 (14) from our conference paper. These results demonstrate that the cheap data from our web supervision method is of sufficient quality to enable models to learn semantic-agnostic forensic features and generalize across unseen real-world IML tasks.

Fig. 12. Qualitative comparison on image manipulation localization.



VIII. CONCLUSION

We propose CAAAv2, a novel category-aware framework that solves the constrained image manipulation localization problem by separately handling Shared Donor Group (SDG) and Shared Probe Group (SPG) image pairs through Difference-Aware Semantic Segmentation and Correlation DINO with frozen DINOv2 backbone, dramatically reducing overfitting while enabling high-quality automatic annotation. With CAAAv2 and a novel metric QES, we auto-annotate manually forged images from the web and harvest a large-scale, diverse, high-quality dataset MIMLv2, comprising 246,212 manually forged images with pixel-level annotations. This dataset considerably addresses the data scarcity issue in IML. Furthermore, we propose Object Jitter, an effective data generation method that leverages authentic web images to improve model performance in challenging cases. To better leverage web-scale supervision, we also introduce Web-IML, a new model for IML. Experiments confirm the strong generalization ability of our method, which achieves unprecedented performance gains and surpasses previous state-of-the-art methods by significant margins. We believe this work establishes a scalable framework for continuously expanding training data as new manually forged images emerge online. Its universal applicability is demonstrated across multiple benchmarks. This research transforms image forensics, shifting reliance from limited, expensive handcrafted datasets to abundant, continuously growing web resources, thus paving the way for more robust and generalizable IML systems.

REFERENCES

[1] R. Peng, S. Tan, X. Mo, B. Li, and J. Huang, “Employing reinforcement learning to construct a decision-making environment for image forgery localization,” *IEEE Transactions on Information Forensics and Security*, 2024.

[2] Z. Sheng, W. Lu, X. Luo, J. Zhou, and X. Cao, “Sumi-ift: An information-theoretic framework for image forgery localization with sufficiency and minimality constraints,” in *Proceedings of the AAAI Conference on Artificial Intelligence*, vol. 39, no. 1, 2025, pp. 720–728.

[3] L. Zhuo, S. Tan, B. Li, and J. Huang, “Self-adversarial training incorporating forgery attention for image forgery localization,” *IEEE Transactions on Information Forensics and Security*, vol. 17, pp. 819–834, 2022.

[4] J. Zhou, X. Ma, X. Du, A. Y. Alhammedi, and W. Feng, “Pre-training-free image manipulation localization through non-mutually exclusive contrastive learning,” in *Proceedings of the IEEE/CVF International Conference on Computer Vision*, 2023, pp. 22 346–22 356.

[5] C. Qu, Y. Zhong, and L. Jin, “Omni-impl: Towards unified image manipulation localization,” *arXiv preprint arXiv:2411.14823*, 2025.

[6] L. Su, X. Ma, X. Zhu, C. Niu, Z. Lei, and J.-Z. Zhou, “Can we get rid of handcrafted feature extractors? sparsevit: Nonsemantics-centered, parameter-efficient image manipulation localization through sparse-coding transformer,” in *Proceedings of the AAAI Conference on Artificial Intelligence*, vol. 39, no. 7, 2025, pp. 7024–7032.

[7] M.-J. Kwon, S.-H. Nam, I.-J. Yu, H.-K. Lee, and C. Kim, “Learning jpeg compression artifacts for image manipulation detection and localization,” *International Journal of Computer Vision*, vol. 130, no. 8, pp. 1875–1895, 2022.

[8] G. Mahfoudi, B. Tajini, F. Reira, F. Morain-Nicolier, J. L. Dugelay, and M. Pic, “Defacto: Image and face manipulation dataset,” in *2019 27th european signal processing conference (EUSIPCO)*. IEEE, 2019, pp. 1–5.

[9] P. Zhou, X. Han, V. I. Morariu, and L. S. Davis, “Learning rich features for image manipulation detection,” in *Proceedings of the IEEE conference on computer vision and pattern recognition*, 2018, pp. 1053–1061.

[10] F. Guillaro, D. Cozzolino, A. Sud, N. Dufour, and L. Verdoliva, “TruFor: Leveraging all-round clues for trustworthy image forgery detection and localization,” in *Proceedings of the IEEE/CVF Conference on Computer Vision and Pattern Recognition*, 2023, pp. 20 606–20 615.

[11] Y. Liu and X. Zhao, “Constrained image splicing detection and localization with attention-aware encoder-decoder and atrous convolution,” *IEEE Access*, vol. 8, pp. 6729–6741, 2020.

[12] S. Xu, S. Lv, Y. Liu, C. Xia, and N. Gan, “Scale-adaptive deep matching network for constrained image splicing detection and localization,” *Applied Sciences*, vol. 12, no. 13, p. 6480, 2022.

[13] M. Oquab, T. Darcet, T. Moutakanni, H. Vo, M. Szafraniec, V. Khalidov, P. Fernandez, D. Haziza, F. Massa, A. El-Nouby *et al.*, “Dinov2: Learning robust visual features without supervision,” *arXiv preprint arXiv:2304.07193*, 2023.

[14] C. Qu, Y. Zhong, C. Liu, G. Xu, D. Peng, F. Guo, and L. Jin, “Towards modern image manipulation localization: A large-scale dataset and novel methods,” in *Proceedings of the IEEE/CVF Conference on Computer Vision and Pattern Recognition*, 2024, pp. 10 781–10 790.

[15] Z. Yu, J. Ni, Y. Lin, H. Deng, and B. Li, “DiffForensics: Leveraging diffusion prior to image forgery detection and localization,” in *Proceedings of the IEEE/CVF Conference on Computer Vision and Pattern Recognition*, 2024, pp. 12 765–12 774.

[16] D. Li, J. Zhu, X. Fu, X. Guo, Y. Liu, G. Yang, J. Liu, and Z.-J. Zha, “Noise-assisted prompt learning for image forgery detection and localization,” in *European Conference on Computer Vision*. Springer, 2024, pp. 18–36.

[17] Z. Zhang, M. Li, X. Li, M.-C. Chang, and J.-W. Hsieh, “Image manipulation detection with implicit neural representation and limited supervision,” in *European Conference on Computer Vision*. Springer, 2024, pp. 255–273.

[18] X. Liu, Y. Yang, H. Wang, Q. Ying, Z. Qian, X. Zhang, and S. Li, “Multi-view feature extraction via tunable prompts is enough for image manipulation localization,” in *Proceedings of the 32nd ACM International Conference on Multimedia*, 2024, pp. 9999–10007.

[19] Y. Liu, S. Chen, H. Shi, X.-Y. Zhang, S. Xiao, and Q. Cai, “Mun: Image forgery localization based on m3 encoder and un decoder,” in *Proceedings of the AAAI Conference on Artificial Intelligence*, vol. 39, no. 6, 2025, pp. 5685–5693.

[20] C. Dong, X. Chen, R. Hu, J. Cao, and X. Li, “Mvss-net: Multi-view multi-scale supervised networks for image manipulation detection,” *IEEE Transactions on Pattern Analysis and Machine Intelligence*, vol. 45, no. 3, pp. 3539–3553, 2022.

[21] K. Zeng, R. Cheng, W. Tan, and B. Yan, “Mgqformer: Mask-guided query-based transformer for image manipulation localization,” in *Proceedings of the AAAI Conference on Artificial Intelligence*, vol. 38, no. 7, 2024, pp. 6944–6952.

- [22] J. Wang, Z. Wu, J. Chen, X. Han, A. Shrivastava, S.-N. Lim, and Y.-G. Jiang, "Objectformer for image manipulation detection and localization," in *Proceedings of the IEEE/CVF Conference on Computer Vision and Pattern Recognition*, 2022, pp. 2364–2373.
- [23] X. Guo, X. Liu, Z. Ren, S. Grosz, I. Masi, and X. Liu, "Hierarchical fine-grained image forgery detection and localization," in *Proceedings of the IEEE/CVF conference on computer vision and pattern recognition*, 2023, pp. 3155–3165.
- [24] Z. Lou, G. Cao, K. Guo, L. Yu, and S. Weng, "Exploring multi-view pixel contrast for general and robust image forgery localization," *IEEE Transactions on Information Forensics and Security*, 2025.
- [25] C. Kong, A. Luo, S. Wang, H. Li, A. Rocha, and A. C. Kot, "Pixel-inconsistency modeling for image manipulation localization," *IEEE Transactions on Pattern Analysis and Machine Intelligence*, 2025.
- [26] Y. Wu, W. Abd-Almageed, and P. Natarajan, "Deep matching and validation network: An end-to-end solution to constrained image splicing localization and detection," in *Proceedings of the 25th ACM international conference on Multimedia*, 2017, pp. 1480–1502.
- [27] Y. Tan, Y. Li, L. Zeng, J. Ye, X. Li *et al.*, "Multi-scale target-aware framework for constrained image splicing detection and localization," *arXiv preprint arXiv:2308.09357*, 2023.
- [28] H. Wu, J. Zhou, J. Tian, and J. Liu, "Robust image forgery detection over online social network shared images," in *Proceedings of the IEEE/CVF Conference on Computer Vision and Pattern Recognition*, 2022, pp. 13 440–13 449.
- [29] N. Otsu, "A threshold selection method from gray-level histograms," *IEEE transactions on systems, man, and cybernetics*, vol. 9, no. 1, pp. 62–66, 1979.
- [30] C. Qu, J. Liu, H. Chen, B. Yu, J. Liu, W. Wang, and L. Jin, "Textsleuth: Towards explainable tampered text detection," *arXiv preprint arXiv:2412.14816*, 2024.
- [31] J. Dong, W. Wang, and T. Tan, "Casia image tampering detection evaluation database," in *2013 IEEE China Summit and International Conference on Signal and Information Processing*, 2013, pp. 422–426.
- [32] A. Novozamsky, B. Mahdian, and S. Saic, "Imd2020: A large-scale annotated dataset tailored for detecting manipulated images," in *Proceedings of the IEEE/CVF Winter Conference on Applications of Computer Vision (WACV) Workshops*, March 2020.
- [33] Reddit, "Photoshopbattles," <https://www.reddit.com/r/photoshopbattles/>.
- [34] B. Wen, Y. Zhu, R. Subramanian, T.-T. Ng, X. Shen, and S. Winkler, "Coverage — a novel database for copy-move forgery detection," in *2016 IEEE International Conference on Image Processing (ICIP)*, 2016, pp. 161–165.
- [35] H. Guan, M. Kozak, E. Robertson, Y. Lee, A. N. Yates, A. Delgado, D. Zhou, T. Kheyrkhah, J. Smith, and J. Fiscus, "Mfc datasets: Large-scale benchmark datasets for media forensic challenge evaluation," in *2019 IEEE Winter Applications of Computer Vision Workshops (WACVW)*. IEEE, 2019, pp. 63–72.
- [36] M. Huh, A. Liu, A. Owens, and A. A. Efros, "Fighting fake news: Image splice detection via learned self-consistency," in *Proceedings of the European Conference on Computer Vision (ECCV)*, September 2018.
- [37] X. Liu, Y. Liu, J. Chen, and X. Liu, "Psc-net: Progressive spatio-channel correlation network for image manipulation detection and localization," *IEEE Transactions on Circuits and Systems for Video Technology*, vol. 32, no. 11, pp. 7505–7517, 2022.
- [38] A. Kirillov, E. Mintun, N. Ravi, H. Mao, C. Rolland, L. Gustafson, T. Xiao, S. Whitehead, A. C. Berg, W.-Y. Lo *et al.*, "Segment anything," in *Proceedings of the IEEE/CVF international conference on computer vision*, 2023, pp. 4015–4026.
- [39] C. Qu, Y. Zhong, F. Guo, and L. Jin, "Revisiting tampered scene text detection in the era of generative ai," in *Proceedings of the AAAI Conference on Artificial Intelligence*, vol. 39, no. 1, 2025, pp. 694–702.
- [40] Z. Zhang, M. Li, and M.-C. Chang, "A new benchmark and model for challenging image manipulation detection," in *Proceedings of the AAAI Conference on Artificial Intelligence*, vol. 38, no. 7, 2024, pp. 7405–7413.
- [41] K. Kadam, S. Ahirrao, K. Kotecha, and S. Sahu, "Detection and localization of multiple image splicing using mobilenet v1," *IEEE Access*, vol. 9, pp. 162 499–162 519, 2021.
- [42] Y. Wu, W. AbdAlmageed, and P. Natarajan, "Mantra-net: Manipulation tracing network for detection and localization of image forgeries with anomalous features," in *Proceedings of the IEEE/CVF Conference on Computer Vision and Pattern Recognition*, 2019, pp. 9543–9552.
- [43] X. Bi, Y. Wei, B. Xiao, and W. Li, "Rru-net: The ringed residual u-net for image splicing forgery detection," in *Proceedings of the IEEE/CVF Conference on Computer Vision and Pattern Recognition Workshops*, 2019, pp. 0–0.
- [44] W. Liu, X. Shen, C.-M. Pun, and X. Cun, "Explicit visual prompting for low-level structure segmentations," in *Proceedings of the IEEE/CVF Conference on Computer Vision and Pattern Recognition*, 2023, pp. 19 434–19 445.
- [45] X. Hu, Z. Zhang, Z. Jiang, S. Chaudhuri, Z. Yang, and R. Nevatia, "Span: Spatial pyramid attention network for image manipulation localization," in *Computer Vision—ECCV 2020: 16th European Conference, Glasgow, UK, August 23–28, 2020, Proceedings, Part XXI 16*. Springer, 2020, pp. 312–328.
- [46] D. Li, J. Zhu, M. Wang, J. Liu, X. Fu, and Z.-J. Zha, "Edge-aware regional message passing controller for image forgery localization," in *Proceedings of the IEEE/CVF Conference on Computer Vision and Pattern Recognition*, 2023, pp. 8222–8232.
- [47] S. Li, W. Ma, J. Guo, S. Xu, B. Li, and X. Zhang, "Unionformer: Unified-learning transformer with multi-view representation for image manipulation detection and localization," in *Proceedings of the IEEE/CVF Conference on Computer Vision and Pattern Recognition*, 2024, pp. 12 523–12 533.
- [48] Y. Wang, Z. Huang, and X. Hong, "Opensdi: Spotting diffusion-generated images in the open world," in *Proceedings of the IEEE/CVF Conference on Computer Vision and Pattern Recognition (CVPR)*, 2025.
- [49] T.-Y. Lin, M. Maire, S. Belongie, J. Hays, P. Perona, D. Ramanan, P. Dollár, and C. L. Zitnick, "Microsoft coco: Common objects in context," in *Computer Vision—ECCV 2014: 13th European Conference, Zurich, Switzerland, September 6–12, 2014, Proceedings, Part V 13*. Springer, 2014, pp. 740–755.
- [50] Z. Liu, H. Mao, C.-Y. Wu, C. Feichtenhofer, T. Darrell, and S. Xie, "A convnet for the 2020s," in *Proceedings of the IEEE/CVF conference on computer vision and pattern recognition*, 2022, pp. 11 976–11 986.
- [51] Y. Liu, X. Zhu, X. Zhao, and Y. Cao, "Adversarial learning for constrained image splicing detection and localization based on atrous convolution," *IEEE Transactions on Information Forensics and Security*, vol. 14, no. 10, pp. 2551–2566, 2019.
- [52] K. Simonyan and A. Zisserman, "Very deep convolutional networks for large-scale image recognition," *arXiv preprint arXiv:1409.1556*, 2014.
- [53] E. J. Hu, Y. Shen, P. Wallis, Z. Allen-Zhu, Y. Li, S. Wang, L. Wang, W. Chen *et al.*, "Lora: Low-rank adaptation of large language models," *ICLR*, vol. 1, no. 2, p. 3, 2022.
- [54] K. Ji, F. Chen, X. Guo, Y. Xu, J. Wang, and J. Chen, "Uncertainty-guided learning for improving image manipulation detection," in *Proceedings of the IEEE/CVF international conference on computer vision*, 2023.
- [55] Z. Zhang, H. Cai, and S. Han, "Efficientvit-sam: Accelerated segment anything model without performance loss," in *Proceedings of the IEEE/CVF Conference on Computer Vision and Pattern Recognition*, 2024, pp. 7859–7863.
- [56] A. Radford, J. W. Kim, C. Hallacy, A. Ramesh, G. Goh, S. Agarwal, G. Sastry, A. Askell, P. Mishkin, J. Clark *et al.*, "Learning transferable visual models from natural language supervision," in *International conference on machine learning*. PmLR, 2021, pp. 8748–8763.
- [57] M. Caron, H. Touvron, I. Misra, H. Jégou, J. Mairal, P. Bojanowski, and A. Joulin, "Emerging properties in self-supervised vision transformers," in *Proceedings of the IEEE/CVF international conference on computer vision*, 2021, pp. 9650–9660.
- [58] Alibaba Security, "Security ai challenger program," <https://tianchi.aliyun.com/competition/entrance/531812/introduction>, 2020.
- [59] P. Zhuang, H. Li, S. Tan, B. Li, and J. Huang, "Image tampering localization using a dense fully convolutional network," *IEEE Transactions on Information Forensics and Security*, vol. 16, pp. 2986–2999, 2021.
- [60] J. Deng, W. Dong, R. Socher, L.-J. Li, K. Li, and L. Fei-Fei, "Imagenet: A large-scale hierarchical image database," in *2009 IEEE conference on computer vision and pattern recognition*. Ieee, 2009, pp. 248–255.
- [61] F. F. Niloy, K. K. Bhaumik, and S. S. Woo, "Cfl-net: Image forgery localization using contrastive learning," in *Proceedings of the IEEE/CVF winter conference on applications of computer vision*, 2023.
- [62] C. Qu, C. Liu, Y. Liu, X. Chen, D. Peng, F. Guo, and L. Jin, "Towards robust tampered text detection in document image: New dataset and new solution," in *Proceedings of the IEEE/CVF Conference on Computer Vision and Pattern Recognition*, 2023, pp. 5937–5946.
- [63] L. Dong, W. Liang, and R. Wang, "Robust text image tampering localization via forgery traces enhancement and multiscale attention," *IEEE Transactions on Consumer Electronics*, 2024.
- [64] B. Zhou, H. Zhao, X. Puig, S. Fidler, A. Barriuso, and A. Torralba, "Scene parsing through ade20k dataset," in *Proceedings of the IEEE conference on computer vision and pattern recognition*, 2017, pp. 633–641.